Heat Transfer Problems Induced By Multi-shocks Interaction

Zonglin JIANG[a,] * and Jingping LI[a]

[a]*Laboratory of High Temperature Gasdynamics, Chinese Academy of Sciences*
Institute of Mechanics, CAS, 15 Beisihuanxilu, Beijing 100190, China
**Email:zljiang@imech.ac.cn*

Abstract. Numerical simulations of the multi-shock interactions observable around hypersonic vehicles were carried out by solving Navier-Stokes equations with the AUSMPW scheme and the new type of the IV interaction created by two incident shock waves was investigated in detail. Numerical results show that the intersection point of the second incident shock with the bow shock plays important role on the flow pattern, peak pressures and heat fluxes. In the case of two incident shocks interacting with the bow shock at the same position, the much higher peak pressure and more severe heat transfer rate are induced than the classical IV interaction. The phenomenon is referred to as the multi-shock interaction and higher requirements will be imposed on thermal protection systems.

Keywords: Heat transfer, Hypersonic flow, Multi-shock interaction, Thermal protection.
PACS: 47.70.Nd

INTRODUCTION

Shock/shock interaction in hypersonic flows has been known as a classic problem arising from incident-shock/bow-shock interactions which will cause extremely high heat transfer rates in the area nearby intersection points for several decades and results in a severe issue for the thermal protection system of hypersonic vehicles. The problem was investigated extensively in the past and six types of the interference patterns were identified according to Edney's classification among which the type IV is considered as the one resulting in the most severe aero-thermal load[1-4]. For hypersonic vehicles powered by air-breathing propulsion, similar, but more complex phenomenon may be observable at the intake cowl lip in which the shock from the vehicle noise and the one generated due to boundary layer separation from vehicle compression surface can intersects with the bow shock of the cowl at the same position since the concept of wave rider or lift body was often applied to enhance vehicle performances. This phenomenon can be referred to as multi-shocks interaction and may be also observable at the leading edge of wings and fins because the boundary separation from vehicle fuselages may induce another shock. Being similar to the classical IV interaction, the multi-shock interaction can induce the much higher peak pressure and more severe heat transfer problem, therefore, the prediction of the resulting heat flux becomes a new critical issue for the TPS design of hypersonic vehicles.

In order to understand the shock dynamic phenomenon, many experimental researches[1-3] were conducted, and the peak pressure, heat transfer rates and its distributions were demonstrated to be sensitive to many factors, such as free flow conditions, shock strength and shock incident angles. Edney[4] and Keyes[5] successfully predicted shock interference patterns, the pressure peak and the heat transfer rate by using oblique shock waves and Prandtl-Meyer expansion relationships. However, in their prediction, the shock standoff distance and transmitted shock length must be known previously. As the development of high resolution schemes proceeds, the complicated shock/shock interactions in hypersonic flows can be investigated by solving Navier-Stokes equations [6-8]. Most of numerical research work was focused on the interaction a single incident shock wave with a bow shock and a lot of flowfield information was provided for designing thermal protection systems. However, it could be more common for hypersonic vehicles powered by air-breathing propulsion that the multi-shock interaction can be created by several incident shock waves because of the boundary layer development and separation. Wieting[9] reported some experiments on the shock interaction of two incident shock waves and more complicated flowfield structures are

CP1233 *The 2nd International ISCM Symposium and The 12th International EPMESC Conference*
J. W. Z. Lu, A.Y.T. Leung, V. P. Iu, and K. M. Mok

reported according to their experimental data. The objective of the present paper is to investigate further into the multi-shock interaction, especially the interaction created by two incident shock waves, at various flow conditions to gain a better understanding on both flow physics and heat transfer.

THE PROBLEM DESCRIPTIONS

Following the classification of Edney, there are six types of shock wave interference patterns when single oblique shock wave intersects the bow shock wave ahead of a blunt body, all of which can occur depending on the strength and relative directions of the intersecting shock waves. Among these types, the type IV is the most severe one that causes the aerothermal loads achieving the highest intensity at the wall, which is the focus in this paper. The type IV interference pattern, as shown in FIGURE 1, occurs when an oblique shock wave intersects the nearly normal part of the bow shock wave ahead of the cylinder. The interaction results in further displacement of the bow shock wave and the formation of a supersonic jet contained between two shear layers. A jet bow shock is produced when the jet impinges on the surface, creating a small region of stagnation heating. The maximum pressure and heat transfer rate occur when the jet impinges perpendicularly to the surface.

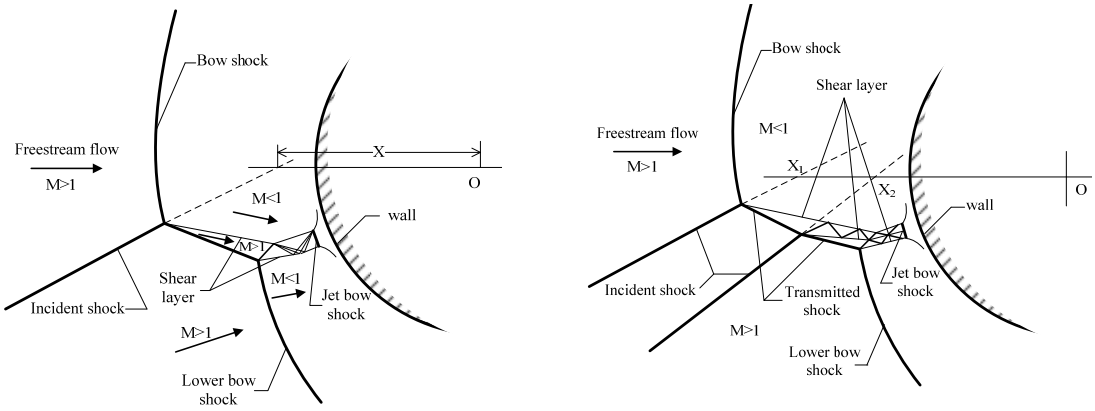

(a) (b)

FIGURE 1. schematic of IV interaction and multi-shock interaction

GOVERNING EQUATIONS AND NUMERICAL METHOD

Assuming that flows is laminar in the present study, the two-dimensional compressible Navier-Stokes equations are accepted as governing equations, written in conservation form of

$$\frac{\partial U}{\partial t}+\nabla\cdot\left(F_I+F_V\right)=0 \tag{1}$$

with

$$U=[\rho,\rho u,\rho v,E]^T$$

where U is the vector of conserved variables, defined in terms of the density ρ, the fluid velocity, u and v, and the total energy per unit mass E that is the sum of the specific internal energy e and the specific kinetic energy of the fluid:

$$E=e+\frac{1}{2}\left(u^2+v^2\right) \tag{2}$$

The convective and viscosity terms are calculated separately with

$$F_I=\begin{pmatrix}\rho u\\ \rho u^2+p\\ \rho uv\\ \rho uE+up\end{pmatrix}i+\begin{pmatrix}\rho v\\ \rho uv\\ \rho v^2+p\\ \rho uE+vp\end{pmatrix}j,\ F_v=\begin{pmatrix}0\\ \tau_{xx}\\ \tau_{xy}\\ u\tau_{xx}+v_{xy}\tau_{xy}-q_x\end{pmatrix}i+\begin{pmatrix}0\\ \tau_{xy}\\ \tau_{yy}\\ u\tau_{xy}+v_{xy}\tau_{yy}-q_x\end{pmatrix}j$$

where p is the pressure, and

$$\tau_{xx} = -\frac{2}{3}\mu\left[\left(u_x + v_y\right) - 3u_x\right] \tag{3}$$

$$\tau_{yy} = -\frac{2}{3}\mu\left[\left(u_x + v_y\right) - 3u_y\right] \tag{4}$$

$$\tau_{xy} = -\mu\left(u_x + v_y\right) = \tau_{yx} \tag{5}$$

The heat flux vector is defined by

$$\mathbf{q} = \left(\frac{\mu}{\mathrm{Pr}}\right)\nabla T \tag{6}$$

where μ is the dynamic viscosity, Pr is the Prandtl number, and T is the temperature. In the present work, AUSMPW scheme[10] was employed for the convective terms calculation, and actually it is an improved version of AUSM scheme[11] by introducing a pressure based weight function to overcome the carbuncle phenomenon and the overshoot problems behind a strong shock. For higher accuracy, the MUSCL approach with primitive variables is adopted to interpolate left and right states across a cell interface. Central difference is used for calculating viscous terms. No-slip boundary conditions are applied at the rigid wall, the pressure is computed by solving a half Riemann problem, and the wall temperature is fixed to 298K..

RESULTS AND DISCUSSION

In this paper, the multi-shock interactions and its influence on aerothermaldynamic loads are investigated with three different cases. The computational conditions for all the cases are listed in Table 1. P_∞, T_∞ and $M\infty$ denote the pressure, the temperature and the Mach number of free stream, respectively. X_1 and X_2 indicate the position of the first incident shock and the second incident shock 2, as shown in FIGURE 1. The radius of the cylinder is R=1.5cm.

TABLE 1. Computational conditions for three test cases

case	P∞	T∞	M∞	Angle of shock 1	Angle of shock 2	X_1	X_2
1	1000Pa	100K	6	22.30	—	-1.35R	—
2	1000Pa	100K	6	14.80	22.30	-1.10R	-1.35R
3	1000Pa	100K	6	14.80	22.30	-1.10R	-0.56R

Classical IV Type Interaction

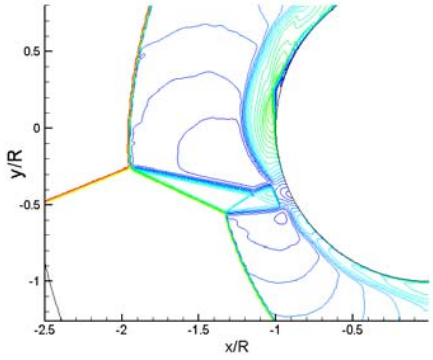

FIGURE 2.a) Mach number contours

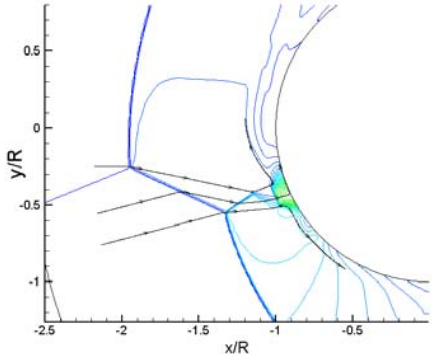

FIGURE 2.b) Pressure contours

It is well known that the type IV, characterized by a supersonic jet that is embedded in a subsonic region, as show in Fig.1, will cause the more severe aerothermal loads at the wall. The type IV interaction is unsteady at a certain level, so, the pressure and heat transfer rate around the cylinder wall are collected after the flow pattern is fully developed with small oscillations of waves around their average positions. Multi-shock interactions are investigated in this paper, but essentially belong to the type IV interaction family. Therefore, classical IV interaction is calculated first as a base for comparison. The grid for cases 2-4 is composed of 300 points in the normal direction and 400 points in the tangential direction, with grid stretching close to the wall and the interaction region. The minimum grid Reynolds number ($\mathrm{Re}_g = \rho_\infty u_\infty \Delta x / \mu_\infty$) at the wall is 5.2.

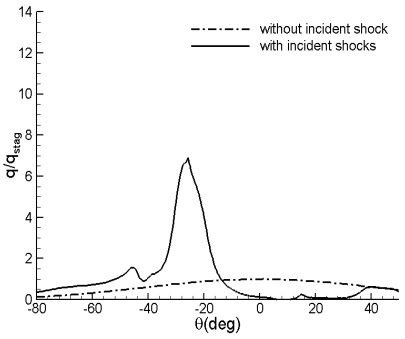

FIGURE 3.a) Distribution of the normalized heat transfer rate around the cylinder wall

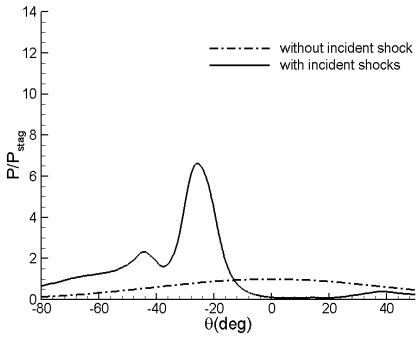

FIGURE 3.b) Distribution of the normalized pressure around the cylinder wall

The classical IV interaction is calculated as the first test case, and the Mach number contours are shown in FIGURE 2A and the pressure contours superimposed with three streamlines are shown in FIGURE 2B. It can be seen that the incident shock intersects the bow shock and a slip line is generated from the triple-point that separates the supersonic region from subsonic region. Another slip line originates is also formed because the transmitted shock interacts with the bow shock. Between the two slip lines there is a supersonic jet in subsonic region, as shown in FIGURE 2A. As the jet approaches the cylinder wall, the supersonic jet is suddenly decelerated through a detached shock and divided into two parts which flow upward and downward from the stagnation point. The peak pressure and the maximum heat transfer rate depend on both the interference pattern and the jet flow angle. For type IV interaction, supersonic jet impinges nearly normally on the cylinder surface, and causes the most severe aerothermal loads. The corresponding heat transfer rate and the pressure normalized by stagnation pressure at the wall are shown in FIGURE 3A and FIGURE 3B, respectively. Their variations and the stagnation point location of the jet agree well with our common understanding.

Multi-shock interactions

The second case is the interaction with two incident shocks. The second incident shock wave interacts with the bow shock at the same position as in case 1, and the first incident shock was located above the second one, but coalesced together before they intersected the bow shock. The computational conditions for this case are given in Table 1.

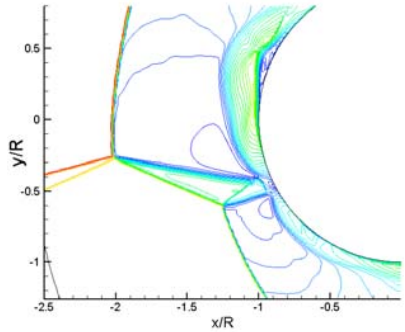

FIGURE 4.a) Mach number contours

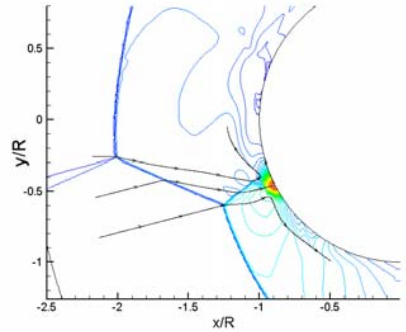

FIGURE 4.b) Pressure contours

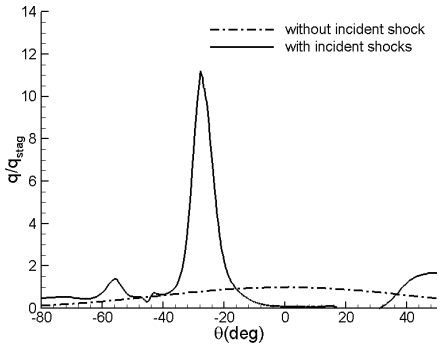

FIGURE 5.a) Distribution of the normalized heat transfer rate around the cylinder wall

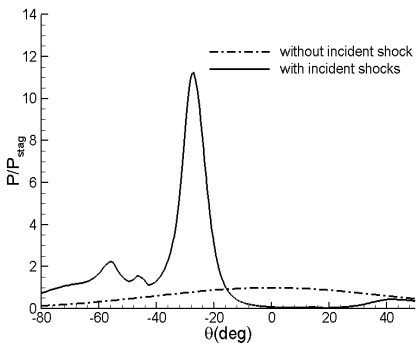

FIGURE 5.b) Distribution of the normalized pressure around the cylinder wall

The Mach number contours and pressure contours are plotted in FIGURE 4A and 4B, respectively. By comparing the flowfield structure with case 1, there is no significant difference observable. Carefully examining shows that the displacement increases slightly for the upper half of the bow shock and decreases for the lower half; the angle of the transmitted shock wave becomes smaller and its strength gets weaker. The supersonic jet is also located in subsonic flows, as shown in FIGURE 4A, therefore, the interference pattern in the second case can be classified as a new type of the IV interaction. However, the supersonic jet is compressed by more oblique shocks and the weaker transmitted shock is developed, which results in total pressure loss decrease and the jet stagnation pressure increase, hence the normalized peak pressure increase remarkably, up to 11.2, as shown in FIGURE 5A. The distribution of normalized heat transfer rate is given in FIGURE 5B, and shows the peak heat transfer rate also increases manifestly and achieves to 11.3. This result can be predicted qualitatively by the theory of Keyes and Hains[5] and the peak value of the heat transfer rate is determined in term of the peak value of pressure.

$$\frac{q_{pk}}{q_{stag}} = 1.03\left(\frac{r}{w_j}\frac{p_{pk}}{p_{stag}}\right)^{\frac{1}{2}} \tag{7}$$

where r is the cylinder radius and w_j the width of the supersonic jet. The formula indicates the peak heat transfer rate is related proportionally with the peak pressure

The third test case is also a multi-shock interaction, but two incident shocks do not coalesced together before they intersected the cylinder bow shock wave. The first incident shock wave was set to be the same to in case 2, and the second incident shock was moved slightly down.

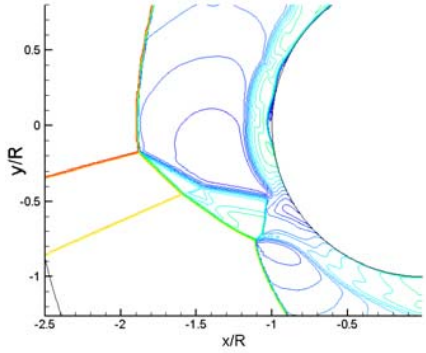

FIGURE 6.a) Mach number contours

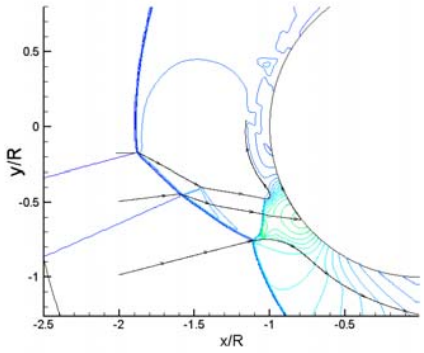

FIGURE 6.b) Pressure contours

The Mach number contours and pressure contours for the third case are shown in FIGURE 6a and 7b. The second incident shock wave intersected the transmitted shock wave created by the first shock and a new shock interference pattern occurred. This new interference pattern, as identified before by Wieting[9], consists of concomitant supersonic jets and a shear layer. From comparison of the results of the third case with case 1, it is obvious that the supersonic jet in this case is wider and shorter, and not perpendicular to the cylinder surface. The stand-off distance of the upper

bow shock decreases and the transmitted shock gets stronger. The pressure and heat transfer rate are plotted respectively in FIGURE 7A and 7B, from which it is observable that both the peak pressure and heat transfer rate decrease to 4.8 and 4.3 respectively. The decreases are quite remarkable.

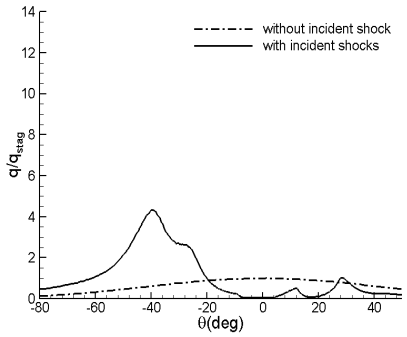

FIGURE 7.a) Distribution of the normalized heat transfer rate around the cylinder wall

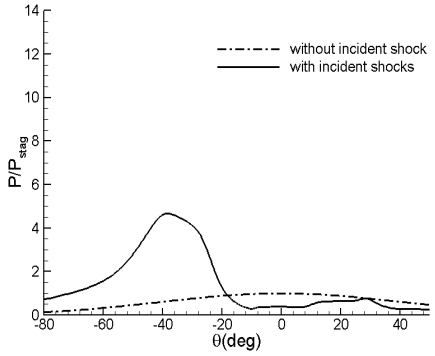

FIGURE 7.b) Distribution of the normalized pressure around the cylinder wall

Multi-shock interactions investigated with the last two cases indicate that the shock interaction patterns strongly depend on the position of two incident shocks. The peak pressure and the heat transfer rate will increase dramatically if two incident shocks interact with the bow shock at the same location.

CONCLUSION

Multi-shock interactions in hypersonic flow were numerically investigated in this paper and the work was dedicated to the new type of the IV interaction with dual incident shock waves. There are more complicated flow field structures consisting of two supersonic jets and three shear layers. Shock interaction patterns strongly depend on the position of two incident shocks. The peak pressure and the heat transfer rate will increase dramatically if two incident shocks interact with the bow shock at the same location. Therefore, these maximum aerodynamics parameters at the leading edge can be minimized by compressing the flow through several small wedge angles and avoiding the incident shock waves to coalesce before they interact with the detached bow shock wave.

REFERENCES

1. Wieting A. R., Holden M. S., Experimental shock-wave interference heating on a cylinder at Mach 6 and 8, AIAA Journal, 27(11)(1989) 1557-1565.
2. Boldyrev S., Borovoy V., etc, A Thorough experimental investigation of shock-shock interferences in high Mach number flows, Aerospace Science Technology, 5 (2001) 167–178.
3. Grasso F., Purpura C., Chanetz B., Type III and type IV shock/shock interferences: theoretical and experimental aspects, Aerospace Science and Technology, 7(2003) 93-106.
4. Edney B., Anomalous heat transfer and pressure distributions on blunt bodies at hypersonic speeds in the presence of an impinging shock, The Aeronautical Research Institute of Sweden, Report 115, 1968.
5. Keyes J. W., Hains F. D., Analytical and experimental studies of shock interference heating in hypersonic flow, NASA,TND-7139,1973.
6. Hsu K., Parpia I. H., Simulation of multiple shock-shock interference patterns on a cylindrical leading edge, AIAA Journal, 34(4)(1996) 764-771.
7. D'Ambrosio, D., Numerical prediction of laminar shock-shock interactions in hypersonic Flow, 40(2)(2003) 153.
8. Vemaganti G. R., Laminar and turbulent flow computations of type IV shock-shock interference aerothermal loads using unstructured grids, NASA CR-195008, 1994.
9. Wieting A. R., Multiple shock-shock interference on a cylindrical leading edge, AIAA Journal, 30(8)(1992) 2073-2079.
10. Kim K. H., Rho O. H., An improvement of AUSM schemes by introducing the pressure based weight functions, Computers & fluids, 27(3)(1998) 311-346.
11. Liou M. S., Ten years in the making-AUSM-family, NASA, TM-210997, 2001.
12. Fay J., Riddell F., Theory of stagnation point heat transfer in dissociated air, Journal of Aeronautical Science, 25(2)(1958) 73-85.